Contents lists available at ScienceDirect

Sensors & Actuators: B. Chemical

journal homepage: www.elsevier.com

Compact model and design considerations of an ion-sensitive floating gate FET

Matti Kaisti [a, *], Qi Zhang [b], Kalle Levon [b]

[a] Technology Research Center, University of Turku, Turku 20520, Finland
[b] Department of Chemical and Biomolecular Engineering, New York University, Brooklyn, NY 11201, USA

ARTICLE INFO

Article history:
Received 31 August 2016
Received in revised form 3 October 2016
Accepted 12 October 2016
Available online xxx

Keywords:
ISFET
SPICE
Model
Chemical sensor
pH
Electrofluidic gating

ABSTRACT

A compact model of an ion-sensitive floating gate FET (ISFGFET) is presented. Unlike in the conventional ISFET, the ISFGFET has a dual gate structure, a sensing gate and a control gate. With the interplay between the control gate and the reference electrode the charging of the fluidic part of the sensor can be controlled and the sensing surface can be programmed. We present an intuitive macromodel with SPICE implementation and discuss the fluidic gating, sensitivity, chemical and electrical tuning of the ionic screening layer as well as the methods to combat the limitations such as the dielectric breakdown of the sensing oxide as well as the design trade-offs of the sensor. Additionally the model allows the integration of this new type of chemical sensor to the CMOS design flow. The proposed model relies on experimentally verified site-binding theory and double layer capacitance formulation explaining the interfacial potential. Unlike previous models we created a unified model where the sensing interface and the FET are coupled and the system is solved as such without unnecessary simplifications used earlier. The model validity is verified by comparing the results with well-established ISFET models and with experimental results.

1. Introduction

Transistor based (bio)chemical sensors are promising in sensing applications due to their inherent capability for miniaturization, scalability, low power and portability [1,2]. Bergveld described the ion-sensitive field-effect-transistor (ISFET) in the 1970s over 40 years ago [3]. Since then the FET based sensing research has been successfully used for genome sequencing [4] monitoring polymerase-chain-reaction (PCR) on chip [5] as well as for the detection of intrinsic charge of macromolecules [6]. Additionally interface readout circuits for large scale arrays and feedback circuits enhancing the sensor response have been described [7].

Previous improvement in modeling efforts includes a robust general interface model [8] and an efficiently solvable model with intuitive device description [9] and its extension to biosensing [10]. Most modeling efforts, however, have concentrated on the conventional ISFET structure. We describe a model for an ISFET variant, the ion-sensitive floating gate field-effect transistor (ISFGFET) [11–13] and discuss its behavior in comparison to ISFET. The ISFGFET employs a floating gate (FG) between the sensing gate (SG) and the underlying transistor structure. Additional control gate (CG) is capacitively coupled to the FG. Both gates can be used to modulate the FET channel conductance. A simplified schematic is shown in Fig. 1. The well established ISFET models are based on the site-binding theory accompanied with the double layer theory [14,9]. We follow this approach, but do not make two simplifying assumptions of earlier models. We do not uncouple the electrolyte from the electronics and we treat the two electrolyte capacitances of the Gouy–Chapman–Stern (GCS) model separately. This allows us to compute the charge and the potential at any point in the electrochemical system. The coupling of the electronics to the solution reveals that we can use the CG to control the ionic screening layer, an ability not found in other ISFET structures.

We have described the ISFGFET physical realization [11,12] and discussed the operation of the structure earlier [13]. Here we extend this work by merging the model as such in a compact form in a SPICE simulation tools and further discuss gating abilities and design trade-offs of the device. Similar structures have been described before [15–17], but thorough analysis of the structure nor a robust model has not been presented. Here we present a convenient and easily accessible HSPICE macromodel for the ISFGFET. This allows seamless and simple integration of the chemical interface to the electronic structure with the ability of an easy scaling towards more complicated designs as well as the addition of parasitic effects.

2. Compact model

A simplified ISFGFET illustration is shown in Fig. 2. The device has two gates, the sensing gate (SG) and a control gate (CG) which are capacitively coupled to a common floating gate (FG). The corresponding gate potentials are Ψ_0 for the SG and V_{CG} for the CG. The device operation can be described by considering the FG potential (V_{FG}) of a floating gate FET [18]

$$V_{\mathrm{FG}} = \frac{C_{\mathrm{CG}} V_{\mathrm{CG}} + C_{\mathrm{SG}} \Psi_0}{C_{\mathrm{TOT}}} + \frac{C_{\mathrm{GS}}}{C_{\mathrm{TOT}}} V_S + \frac{C_{\mathrm{DS}}}{C_{\mathrm{TOT}}} V_D + \frac{Q}{C_{\mathrm{TOT}}} \quad (1)$$

and by considering the V_{FG} and drain current I_D relationship of the

* Corresponding author.
Email address: mkaist@utu.fi (M. Kaisti)

http://dx.doi.org/10.1016/j.snb.2016.10.051
0925-4005/

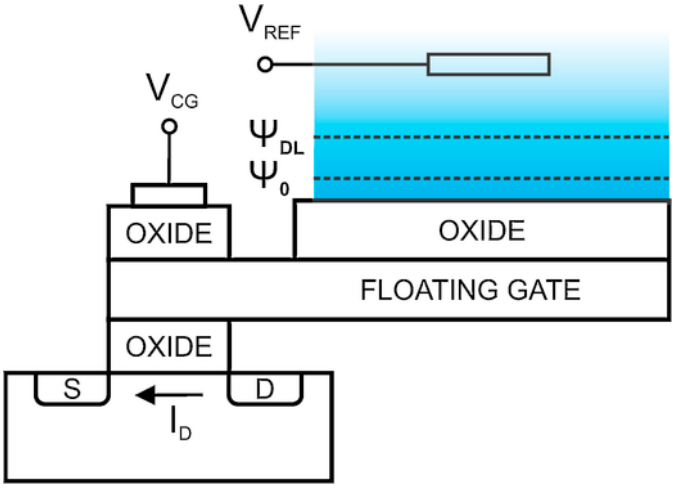

Fig. 1. Simplified ISFGFET schematic. The solution is modeled with Gouy–Chapman–Stern model. The V_{CG} and V_{REF} are the control gate and reference electrode potentials. The Ψ_0 is the surface potential of the oxide and Ψ_{DL} is the potential at the Stern layer.

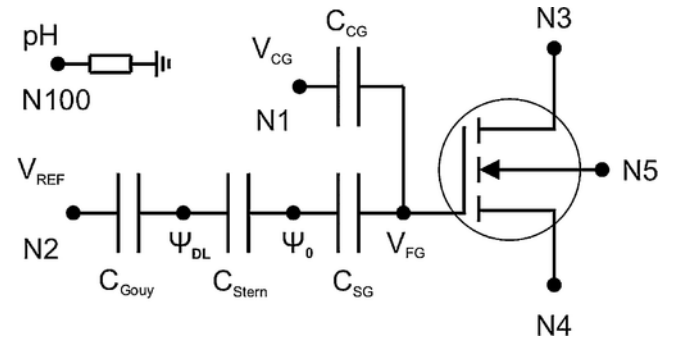

Fig. 2. Macromodel description of the ISFGFET. The model input nodes: N1 is the CG potential (V_{CG} node), N2 is the REF potential (V_{REF} node), N3 is drain voltage (V_D node), N4 is the source voltage (V_S node), N5 is the body terminal of the transistor and N100 is defined as the pH input. The Gouy–Chapman–Stern model defines the capacitors of the double layer and the surface potential of the oxide Ψ_0 and the potential at the Stern layer Ψ_{DL}.

underlying nmos in the linear region

$$I_D = \mu C_{\text{ox}} \frac{W}{L}\left((V_{\text{FG}} - V_{\text{th}})V_{\text{DS}} - \frac{V_{\text{DS}}^2}{2}\right) \quad (2)$$

where V_{th} is the MOSFET threshold voltage, μ_n is the carrier mobility, C_{ox} gate oxide capacitance per unit area, L is the gate width and L is the length. The source node is considered to be grounded. The net charge Q at FG is considered to be zero in the simulations. Deviations from the assumption are seen as constant shifts in the threshold voltage. The parasitic capacitances C_{GS} and C_{GD} where experimentally found to have negligible impact on the device behavior and are thus omitted. These can be easily incorporated in the presented compact model in SPICE. The sensing branch of the ISFGFET consisting of the FG, sensing oxide, electrolyte solution and a reference electrode is modeled with behavioral voltage sources in SPICE. Our definition follows the guidelines presented by Jiang and Stein [19]. In Fig. 2 the ISFGFET macromodel is shown. The electrolyte capacitance is usually much larger than the other series capacitances (sensing layer and FET gate oxide and depletion layer) and thus the coupling of the reference electrode to the sensing gate can be approximated as

$$\Psi_0 = V_{\text{REF}} + V_{\text{cell}}^0 + V_{\text{pH}} \quad (3)$$

where V_{cell}^0 describes the constant interfacial potentials associated to the electrochemical cell and the V_{pH} is the chemically relevant term. This approximation explains the device operation and the voltage sources in series in the electrochemical cell. However, it is clear from the model formulation in Table 1 that the Ψ_0 and V_{pH} are interlinked. Additionally we note that the model assumes that the solution bulk potential equals the V_{REF}. Junction potential corrections can be easily embedded into the V_{REF}.

2.1. Model definition

The model is solved in a HSPICE sub-circuit block. The non-linear equations (7) and (8) in Table 1 are solved using behavioral voltage sources. The FG and CG nodes are capacitively connected to n-type FET and are simulated using standard SPICE circuit elements. The block diagram of the macromodel is shown in Fig. 2. There are six input nodes for the sub-circuit: control gate N1, reference electrode N2, drain N3, source N4, bulk N5 and a pH N100. The electrolyte pH has been included as an input node to allow simple simulation of the model for pH changes [9]. Using the model provided in Appendix A other parameters can be included similarly as a sub-circuit input node as well. The Appendix A specifies a user specific proprietary transistor model. In our case it is an nmos transistor comprising eight parallel transistor fingers and a control gate capacitor. The sensor has a pristine threshold voltage of 1 V at the FG. Both the control gate and the gate oxide capacitances are 0.13 pF.

2.2. Device description

The chip was manufactured with 0.25 μm double polysilicon gate CMOS process. It was encapsulated with PDMS to protect the bond-

Table 1
Compact model equations.

$\text{S}\cdot\text{OH} \overset{K_A}{\rightleftharpoons} \text{S}\cdot\text{O}^- + \text{H}_B^+(\text{aq})$	(1)
$\text{S}\cdot\text{OH}_2^+ \overset{K_B}{\rightleftharpoons} \text{S}\cdot\text{OH} + \text{H}_B^+(\text{aq})$	(2)
$\sigma_{SG} = C_{SG}(V_{FG} - \Psi_0)$	(3)
$\sigma_{DL} = C_{Stern}(\Psi_0 - \Psi_{DL})$	(4)
$V_{\text{FG}} = \frac{V_{\text{CG}}C_{\text{CG}} + \Psi_0 C_{\text{SG}}}{C_{\text{TOT}}} + \frac{Q}{C_{\text{TOT}}}$	(5)
$C_{TOT} = C_{CG} + C_{SG} + C_{OX}$	(6)
$\Psi_0 = V_{\text{FG}} + \frac{\sigma_0 - \sigma_{\text{DL}}}{C_{\text{SG}}}$	(7)
$\Psi_{\text{DL}} = \Psi_0 - \frac{\sigma_{\text{DL}}}{C_{\text{stern}}}$	(8)
$\sigma_0 = \frac{-e\Gamma}{1 + \frac{[H_B^+]}{K_A}\exp\left(\frac{-e(\Psi_0 - V_{\text{REF}})}{\text{kT}}\right)} + \frac{e\Gamma}{1 + \frac{K_B}{[H_B^+]}\exp\left(\frac{e(\Psi_0 - V_{\text{REF}})}{\text{kT}}\right)}$	(9)
$\sigma_{\text{DL}} = \frac{2e_w e_0 \text{kT}}{e\lambda_D}\sinh\left(\frac{e(\Psi_{\text{DL}} - V_{\text{REF}})}{2\text{kT}}\right)$	(11)
$\lambda_D = \left(\frac{e_w e_0 \text{kT}}{2z^2 e^2 n_0}\right)^{1/2}$	(12)
$pK_B = -\log_{10}(K_A),\ pK_B = -\log_{10}(K_B)$	(13)
$pH = -\log_{10}([H^+])$	(14)

ing wires. The chip's overall dimensions are 5 mm × 5 mm. The individual sensors were glass passivated during the manufacturing process. The passivation consisted of a 0.5 μm thick SiO_2 layer followed with a 1 μm Si_3N_4 layer deposited on top. The passivation layer was etched using reactive-ion etching (RIE) that exposed the underlying aluminium sensing pads. A thin layer of native Al_2O_3 oxide formed on the surface with an expected thickness of 6 nm.

In Fig. 3(a) the top view of the manufactured chip is shown. In (b) a SEM image of the device illustrates the cross sectional structure. The metal vias from the FG, source and drain nodes to the top of the chip are shown. The figure zooms in and shows two FGs of a single sensor that consists of eight parallel fingers. In (c) a sensing pad SEM image is shown and (d) is the top view of the layout indicating the positioning of the sensing pad compared to the underlying electrical structure. The pad is not directly on top of the transistor minimizing the effect of the parasitic capacitances.

3. Results and discussion

3.1. Capacitive attenuation

Aside from the surface pH sensitivity the underlying sensor has a significant impact on how strongly this potential change is seen in the drain current. The capacitive network that capacitively connects the two inputs to the FG has a strong influence to the behavior of the sensor. Both sensor input nodes, the control gate and the sensing gate, can be used to modulate the sensor drain current. Thus the sensor has two sensitivities defined as a change in output per unit change at one of the inputs, V_{CG} or Ψ_0. The change in the V_{FG} resulting from the inputs is given as

$$\Delta V_{\mathrm{FG}} = \frac{C_{\mathrm{CG}}}{C_{\mathrm{TOT}}}\Delta V_{\mathrm{CG}} + \frac{C_{\mathrm{SG}}}{C_{\mathrm{TOT}}}\Delta\Psi_0 \tag{4}$$

where $C_{TOT} = C_{CG} + C_{SG} + C_{OX}$. The sensing gate surface potential is weighted with a capacitive ratio that is always less than one, limiting its sensitivity.

In [13] we described the general behavior of the device concentrating on the relationships between the sensing oxide and the electrolyte solution. Here we extend this work with a fully merged SPICE model and consider the practical abilities of the sensor in terms of V_{CG}. We elaborate the sensor behavior in following simulations where we fixed the CG and SG capacitances to be roughly the same, larger than C_{OX}, but smaller than the double layer capacitance of the solution. Therefore the capacitive ratio in Eq. (4) for both sensitivities is ≈0.5.

3.2. Electrofluidic gating

The ability to probe the ionic screening layer with electrostatic force is called electrofluidic gating [19]. In our device the V_{FG} can be controlled through the CG. This changes the potential across the sensing oxide and subsequently across the solution allowing the programming of the sensing gate and the fluidic part of the device.

The sensing surface with ionizable surface groups acts as buffer when potential changes at the FG. This buffering capability is strongly depended on the density of these groups [19]. In Fig. 4(a) the relationship between surface potential and the sensing gate oxide field strength is shown. With high density of ionizable groups the ionic screening layer charge remains practically unaffected. There is an abundance of ionizable groups that respond to the applied electric field by either protonating or deprotonating leaving the surface potential unaffected. On the other extreme are surfaces with no ionizable groups. Then the charging follows linearly the changes in the oxide field strength as shown in (c). This is due to the counter-ions in the double layer completely screening the field induced surface charging i.e. the lost ability to buffer against the changes in charging at the surface. In between, we have surfaces with limited buffering capacity where the surfaces act as a buffer with modest field strengths. With increased fields the curves run in parallel with the inert surface indicating and that all ionizable groups have responded. The figures (b)

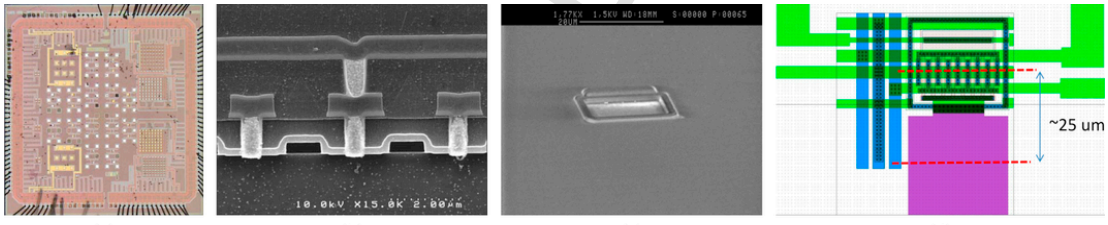

Fig. 3. (a) Top view of the ISFGFET chip. (b) Cross-sectional SEM image of the sensor showing two floating gates of a single sensor. (c) SEM image of the sensing area and (d) a top-view layout indicating the sensing area placement in relation to the underlying device structure.

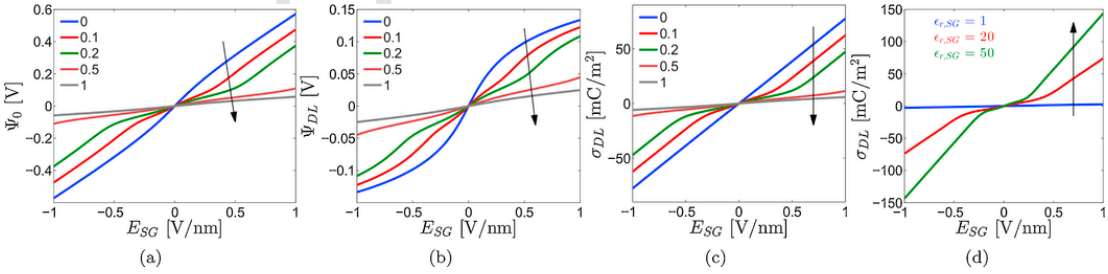

Fig. 4. (a) The surface potential Ψ_0, (b) double layer potential Ψ_{DL} and (c) the double layer charge σ_{DL} response to varying E_{SG} with different N_S in units of nm^{-2}. Surface dissociation constants are $pK_A = 8$ and $pK_B = 6$ and the solution pH is 7. In all cases the V_{REF} is considered grounded and c = 10 mM. (d) is as (c) but with different values of sensing oxide dielectric constants and with $N_S = 0.2$ nm^{-2}.

and (c) show the response in the double layer potential and charge under the same simulation. The pH sensitivity (not shown) goes hand in hand with the buffering capacity. With high ionizable group density the surface exhibits Nernstian response. For field-effect control of the solution a non-Nernstian surface is required with reduced pH sensitivity. A similar observation has been discussed earlier [16].

3.3. Gating enhancement

To have a strong ability for electrofluidic gating the C_{SG} should be large enough that significant coupling of ΔV_{FG} can be seen at the ionic screening layer. Increasing capacitive coupling by scaling the area is limited since both double layer capacitance and C_{SG} capacitance ideally scale directly with it. Non-idealities related to the SG capacitance has been reviewed briefly [13]. Using the dielectric thickness for increased capacitance is limited due to the dielectric breakdown since thicker oxides reduce the coupling strength. The gating ability can be enhanced by increasing the dielectric constant of the sensing oxide. An example is shown in Fig. 4(d). This strategy is limited by the availability of suitable dielectrics, but clear coupling improvements are achievable. This further complicates the design and adds trade-offs with intrigue interplay between the design parameters.

3.4. Chemical and electrical tuning

In Fig. 5 the ability to chemically tune the double layer charging via changing the solution pH (a) or the surface dissociation constants (b) is shown. The charging in both cases is simulated with a sweeping $V_{CG} - V_{REF}$ potential difference. The change of pH shifts the curves as it directly changes the charging in the surface and thus in the ionic screening layer. An analogous effect shown in Fig. 5(b) can be achieved by adjusting the surface dissociation constants. The strongest change due to an applied field in the surface charging happens when the pK value is close to the pH of the electrolyte solution. Commonly this means that only one of the groups is buffering when the other group remains mostly protonated or deprotonated. Thus, the pH and surface pK values are interlinked. With lower pK values the double layer becomes relatively more negatively charged since the PZC lies at a lower pH. The simulations consider changing the V_{CG}, but as the charging at the sensing branch is determined by the potential difference between V_{FG} and V_{REF} the interplay with the reference electrode can be used for fluidic gating while controlling the FET bias point independently.

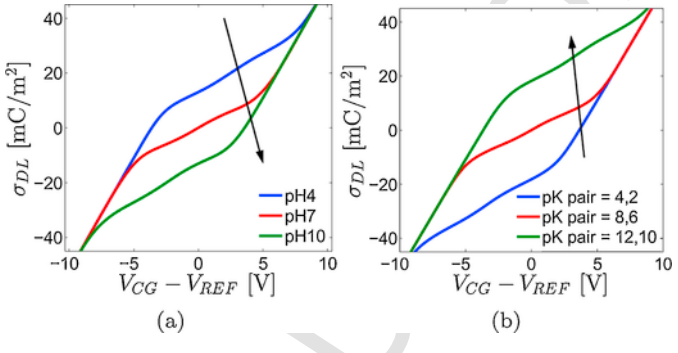

Fig. 5. Chemical and electrical tuning of the surface. (a) Electrolyte pH is varied with $pK_A = 8$ and $pK_B = 6$. (b) Surface dissociation constants are varied in pH = 7. In both cases the V_{REF} is considered grounded, c = 10 mM and $N_S = 0.2$ nm^{-2}.

3.4.1. Salinity

The salinity of the electrolyte has a strong impact on the ionic screening length defined via the Debye screening length (Eq. (12) in Table 1). Increasing the salinity decreases ionic screening length and increases the diffuse layer capacitance. With small salt concentration the double layer capacitance is decreased and the potential difference increasingly falls on the solution and the diffuse layer. This indicates stronger changes in the oxide and the ionic screening layer potentials with lowering salt concentration as is observed in Fig. 6(a). However, the ionic screening layer charge in (b) remains static (while sweeping V_{CG}) within the buffering regime when the salt concentration is low. This is because the diffuse layer with smaller capacitance, requires smaller charge density changes for compensating the potential changes at the sensing surface.

3.5. Model verification

We compare the pH sensitivity of our macromodel with the model by van Hal et al. [14,8]. The model described by van Hall et al. considers the electrolyte solution being uncoupled from the transistor. We do not make such simplification and additionally we separate the combined Stern layer and diffuse layer capacitances allowing computation of the screening layer potential and charge. We computed the pH response with Al_2O_3 and Ta_2O_5 surfaces using both models and compared them in the same setting. In the ISFET model by Van Hall et al. the underlying transistor has no influence as it is uncoupled from the solution. In our ISFGFET model the potential at the FG influences the surface potential. To allow best comparison of the surface behavior between models we connected all transistor nodes to ground. In both simulations the bulk solution potential was set to zero. The pH sensitivity between the models with Al_2O_3 and Ta_2O_5 surfaces are in agreement. In the ISFGFET model the FG, surrounded by capacitive network, is floating. Some of the charge generated by the surface is distributed across the oxide creating a small, but negligible difference between sensitivities. Reported measured results with a commercial Sentron 1090 Al_2O_3 ISFET and a Ta_2O_5 gate ISFET [20] show good agreement with the modeled results as shown in Table 2. A small discrepancy between the measured ISFGFET sensitivity was found in the alkaline end of the pH range where in the acidic range the agreement is good as shown in Fig. 7(a).

The model estimates the pH sensitivity accurately, but it can also predict the entire device behavior in absolute terms. Fig. 7(b) shows the simulated and measured transfer curves of the electrical part of the sensor when the V_{CG} is swept and I_D is measured. This measurement checks the validity of the underlying transistor SPICE model. In Fig. 7(b) the transistor is measured in dry conditions. The SG is float-

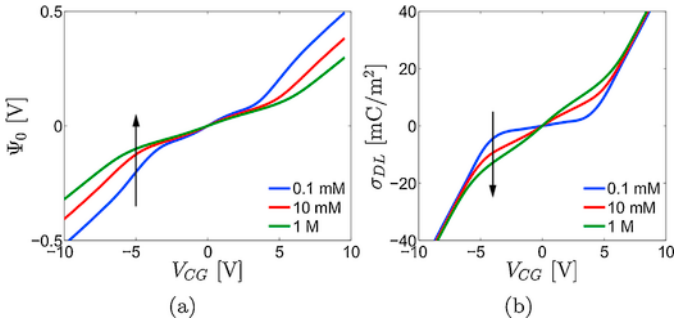

Fig. 6. Impact of salinity. The surface potential (a) and the double layer charge (b) with different monovalent salt concentrations. Electrolyte pH is 7 and $pK_A = 8$ and $pK_B = 6$ with $N_S = 0.2$ nm^{-2}.

Table 2
ISFET sensitivity comparison. Experiments for Al_2O_3 were conducted in pH range 1, …, 13 @ 25 °C and for Ta_2O_5 in pH range 1, …, 10 @ 25 °C [20]. Both models were examined in pH range 1, …, 14 in 1 M solution with Stern capacitance 18 μF/cm^2.

	Sensitivity [mV/pH]			
Gate material	ISFET model [14]	ISFGFET macromodel	ISFET measured [20]	ISFGFET measured [13]
Al_2O_3	53.0	53.2	53.2	50.9
Ta_2O_5	58.5	58.6	59.4	

ing and does contribute to the obtained responses. The SPICE model predicts fairly well the measured behavior, but the measured current is on average approximately 1.2 times larger than the simulated current. We use this factor to correct the MOSFET gate voltage and I_D relationship of the foundry specific SPICE model by multiplying the model I_D with it. We are unable to directly probe the mismatch between the MOSFET gate voltage and drain current relationship since the bias is applied through one of the input gates and a capacitive division between the gate oxide and CG oxide might distort the result. However, such capacitances are usually well defined and moreover, using the same correction corrects the measured drain currents regardless which input gate is used for biasing under different biasing conditions. Therefore we are confident that the used correction of the electrical part is valid.

In Fig. 7(c) the ISFGFET transfer curves are simulated under chemical sensing and compared to the corresponding measurements in buffers solution with pH values 4, 7 and 10. The simulation corresponds well with the measured results. The simulation vs. measurements for two different sensing areas are additionally compared in Fig. 7(d). In both cases the agreement is good. The reduced current is due to the combined effect of capacitive division and the difference in the drain current and V_{FG} relationship between the sensors. Regardless, it further verifies the model validity under different sensing areas.

4. Conclusions

We showed an intuitive model of the ISFET variant, the ISFGFET that possesses some new possibilities unmet in the classical ISFET. In addition to the control of the operation point using the control gate the intrigue interplay between the CG and REF can be used to modulate the solution charging via the field-effect. The model was verified through electrical characterizations and chemical measurements from which transfer curves were extracted. The developed model allows simple incorporation of non-ideal effects such as parasitic capacitances, temperature effects and even temporal drifts. The model allows the incorporation of the device as an electrical circuit element which can be incorporated into CMOS design flow. This allows for example the simulation of various front-end configurations and larger arrays with high computational efficiency.

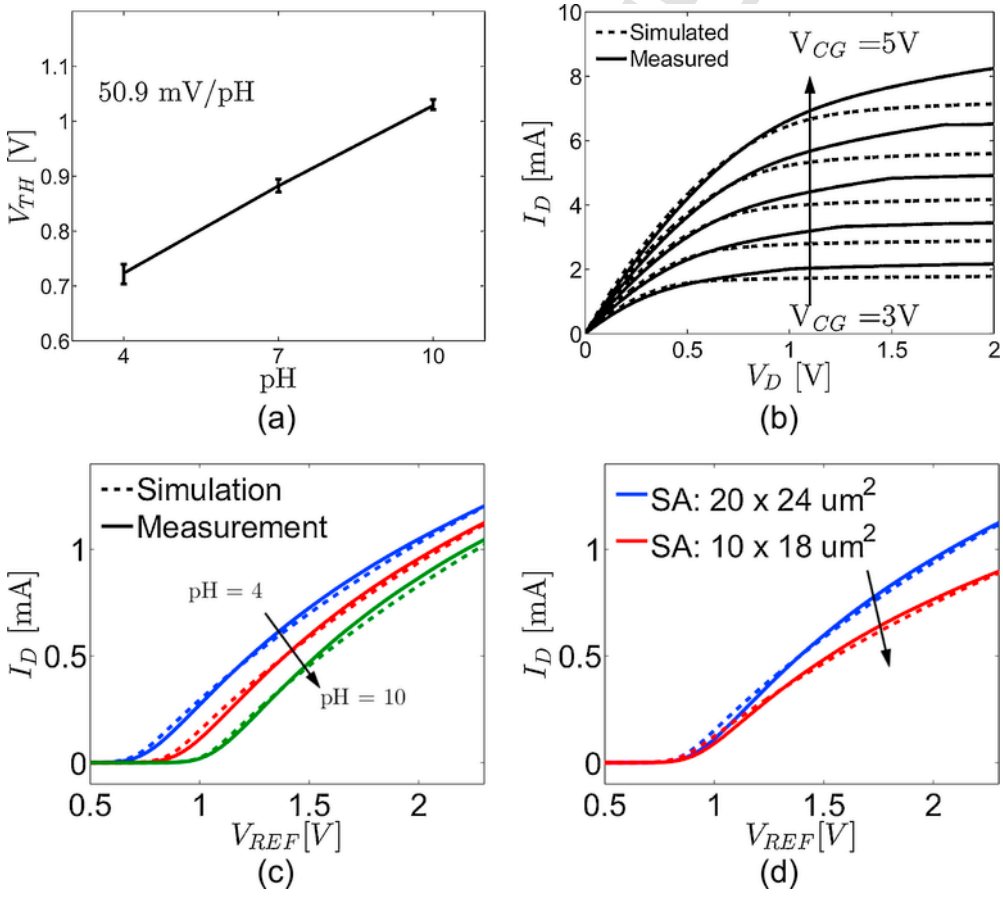

Fig. 7. (a) Measured ISFGFET pH sensitivity. (b) Simulated vs. measured transfer curves of the ISFGFET biased through the control gate while leaving the sensing gate uncoupled. (c) Comparison of the compact model simulation to measurements under buffers with pH values of 4, 7 and 10. (d) Comparison of two individual sensors transfer curves with different area in pH 7 with simulations (dashed line) and measurements (solid line).

Appendix A.

```
.OPTION LIST
+dcstep=1000
+gmindc =1e-24 itl1=1000 converge accurate
+ post=1

.PARAM
+ k = 1.38e-23
+ T = 300
+ q = 1.602e-19
+ Vt = '((k*T)/q)^1'
+ e0 = 8.85e-12
+ Na = 6.02e23
+ erw = 78.4
+ N = 1e17
+ pKa = 8
+ pKb = 6
+ c = 10e-3
+ pH = 7
+ ero = 9.3
+ d = 10e-9
+ A = 500e-12
+ debye = '((erw*e0*k*T)/(2*q^2*Na*1000*c))^0.5'
+ Cs = '10*e0/5e-10'
+ Csg = 'ero*e0/d'

SUBCIRCUIT DEFINITION
.SUBCKT ISFGFET N1 N2 N3 N4 N5 N100
USER SPESIFIC (NMOS) MODEL

*REMOVAL OF FLOATING NODES
R201 0 N201 1e23
R202 0 N202 1e23

*INTERFACE CAPACITANCES
Cs N201 N202 C = '10*e0/5e-10*A'
Csg N200 N201 C = 'ero*e0/d*A'

*SYSTEM OF NON-LINEAR EQUATIONS
EPC D1 0 VOL = '-q*N/(1 + 10^(pKa - V(N100))*EXP(-Vt*(V(N201)-
V(N2))))'
ENC D2 0 VOL = 'q*N/(1 + 10^(V(N100) - pKb)*EXP(Vt*(V(N201)-
V(N2))))'
EDC D3 0 VOL = '2*erw*e0*k*T/(debye*q)*sinh(Vt*(V(N202)-V(N2))/(2)

E1 N201 0 VOL = 'V(N200) + (V(D1) + V(D2) - V(D3))/Csg'
E2 N202 0 VOL = 'V(N201) - V(D3)/Cs'
.ENDS ISFGFET

*EXAMPLE CIRCUIT
XIS Vcg Vref Vd Vs Vb Vph ISFGFET

VB Vb 0 0
VS Vs 0 0
VDD Vd 0 DC 2
VREF Vref 0 DC 0

*Example
VPH Vph 0 DC 7
VG Vcg 0 PULSE(-15 15 10ns 100ns 100ns 0ns 1000ns)
.TRAN 1ns 110ns START = 10ns SWEEP N POI 5 0e16 1e17 2e17 5e17
1e18

.end
```

References

[1] M.J. Schoning, A. Poghossian, Recent advances in biologically sensitive field-effect transistors (BioFETs), Analyst 127 (2002) 1137–1151.

[2] A. Poghossian, M.J. Schöning, Label-free sensing of biomolecules with field-effect devices for clinical applications, Electroanalysis 26 (6) (2014) 1197–1213, http://dx.doi.org/10.1002/elan.201400073.

[3] P. Bergveld, Thirty years of ISFETOLOGY: what happened in the past 30 years and what may happen in the next 30 years, Sens. Actuators B: Chem. 88 (1) (2003) 1–20, http://dx.doi.org/10.1016/S0925-4005(02)00301-5.

[4] J.M. Rothberg, et al., An integrated semiconductor device enabling non-optical genome sequencing, Nature 475 (2011) 348–352, http://dx.doi.org/10.1038/nature10242.

[5] C. Toumazou, et al., Simultaneous DNA amplification and detection using a pH-sensing semiconductor system, Nat. Methods 10 (2013) 641–646, http://dx.doi.org/10.1038/nmeth.2520.

[6] F. Fixe, H. Branz, N. Louro, V. Chu, D. Prazeres, J. Cond, Immobilization and hybridization by single sub-millisecond electric field pulses, for pixel-addressed DNA microarrays, Biosens. Bioelectron. 19 (12) (2004) 1591–1597, http://dx.doi.org/10.1016/j.bios.2003.12.012.

[7] N. Moser, T.S. Lande, C. Toumazou, P. Georgiou, ISFETs in CMOS and emergent trends in instrumentation: a review, IEEE Sens. J. 16 (17) (2016) 6496–6514, http://dx.doi.org/10.1109/JSEN.2016.2585920.

[8] R. van Hal, J. Eijkel, P. Bergveld, A general model to describe the electrostatic potential at electrolyte oxide interfaces, Adv. Colloid Interface Sci. 69 (1-3) (1996) 31–62.

[9] S. Martinoia, G. Massobrio, A behavioral macromodel of the ISFET in spice, Sens. Actuators B: Chem. 62 (3) (2000) 182–189.

[10] P.G. Fernandes, H.J. Stiegler, M. Zhao, K.D. Cantley, B. Obradovic, R.A. Chapman, H.-C. Wen, G. Mahmud, E.M. Vogel, Spice macromodel of silicon-on-insulator-field-effect-transistor-based biological sensors, Sens. Actuators B: Chem. 161 (1) (2012) 163–170, http://dx.doi.org/10.1016/j.snb.2011.10.002.

[11] K. Levon, A. Rahman, T. Sai, B. Zhao, Floating gate field effect transistors for chemical and/or biological sensing, US Patent 7 462 512 B2 (Dec. 9, 2008).

[12] Q. Zhang, H. Majumdar, M. Kaisti, A. Prabhu, A. Ivaska, R. Osterbacka, A. Rahman, K. Levon, Surface functionalization of ion-sensitive floating-gate field-effect transistors with organic electronics, IEEE Trans. Electron Devices 62 (4) (2015) 1291–1298, http://dx.doi.org/10.1109/TED.2015.2396996.

[13] M. Kaisti, Q. Zhang, A. Prabhu, A. Lehmusvuori, A. Rahman, K. Levon, An ion-sensitive floating gate FET model: operating principles and electrofluidic gating, IEEE Trans. Electron Devices 62 (8) (2015) 2628–2635.

[14] R. van Hal, J. Eijkel, P. Bergveld, A novel description of ISFET sensitivity with the buffer capacity and double-layer capacitance as key parameters, Sens. Actuators B: Chem. 24 (1,3) (1995) 201–205.

[15] N.Y.-M. Shen, Z. Liu, C. Lee, B.A. Minch, E.C.-C. Kan, Charge-based chemical sensors: a neuromorphic approach with chemoreceptive neuron MOS (CvMOS) transistors, IEEE Trans. Electron Devices 50 (10) (2003) 2171–2178.

[16] K. Jayant, K. Auluck, M. Funke, S. Anwar, J.B. Phelps, P.H. Gordon, S.R. Rajwade, E.C. Kan, Programmable ion-sensitive transistor interfaces. I. Electrochemical gating, Phys. Rev. E 88 (2013) 012801, http://dx.doi.org/10.1103/PhysRevE.88.012801.

[17] M. Barbaro, A. Bonfiglio, L. Raffo, A charge-modulated FET for detection of biomolecular processes: conception, modeling, and simulation, IEEE Trans. Electron Devices 53 (1) (2006) 158–166.

[18] T. Shibata, T. Ohmi, A functional MOS transistor featuring gate-level weighted sum and threshold operations, IEEE Trans. Electron Devices 39 (6) (1992) 1444–1455, http://dx.doi.org/10.1109/16.137325.

[19] Z. Jiang, D. Stein, Electrofluidic gating of a chemically reactive surface, Langmuir 26 (11) (2010) 8161–8173, http://dx.doi.org/10.1021/la9044682.

[20] Sensitivity and hysteresis effect in Al_2O_3 gate pH-ISFET, Mater. Chem. Phys. 71 (2) (2001) 120–124, http://dx.doi.org/10.1016/S0254-0584(00)00513-7.

Matti Kaisti received his B.Sc. from Turku University of Applied Sciences in 2008 and his M.Sc. degree in 2012 from University of Turku, both in electrical engineering and the M.Econ degree from the Turku School of Economics in 2016. From 2008 to 2012 he worked as an RF design engineer in DA-Design OY in Finland developing radars and radiometers for environmental applications and also designed several radiometer systems in an ESA research project exploring new technology for future space missions. Currently he is working towards the Ph.D. degree in bio-electronics at University of Turku concentrating on bio(chemical) sensors. His research focuses on field-effect based sensor structures and DNA sensors for medical diagnostics.

Qi Zhang received his B. Eng degree in Materials Science and Engineering from Donghua University in 2008 and his Ph.D. degree in Materials Chemistry from New York University in 2014. He is currently working with a NYC based biotech startup to develop point-of-

care (POC) bio-sensing devices. His research interests include designing and developing functional materials, assays and electrochemical devices for medical diagnostic applications.

Kalle Levon received his BSc and Msc degrees from the University of Helsinki and the doctor degree from the University of Tokyo. He started as a professor at Polytechnic University in 1989 and has since been there the chairman and the vice-provost of research. His research areas focus on non-equilibrium phase separations and organic electronics.